Rapid expansion of fixed nitrogen deficit in the eastern Pacific Ocean revealed by 50 year time series

Natalya Evans[1], Juliana Tichota[1], Wendi Ruef[2], James Moffett[1], and Allan Devol[2]

[1]Department of Biological Sciences, University of Southern California; Los Angeles, California
[2]School of Oceanography, University of Washington; Seattle, Washington.

August 14, 2023

Rapid expansion of fixed nitrogen deficit in the eastern Pacific Ocean revealed by 50-year time series

Natalya Evans[1], Juliana Tichota[1], Wendi Ruef[2], James Moffett[1], and Allan Devol[2]*.

[1]Department of Biological Sciences, University of Southern California; Los Angeles, California.

[2]School of Oceanography, University of Washington; Seattle, Washington.

Corresponding author: Allan Devol (devol@uw.edu)

Key Points:

- The nitrogen deficit in the largest Oxygen Deficient Zone (ODZ) has increased over 50 years, indicating a 30% increase in ODZ strength
- The maximum fixed N loss of the core ODZ (σ_θ 26.2-26.8 kg m^{-3}) is significantly different (p=0.03) from its natural variability
- Though the core ODZ intensification is significant, we cannot yet claim with virtual certainty (p=0.01) that climate change caused it

Abstract

Climate change is expected to increase the strength of ocean Oxygen Deficient Zones (ODZs), but we lack detailed understanding of the temporal or spatial variability of these ODZs. A fifty-year time series in the Eastern Tropical North Pacific (ETNP) ODZ revealed that it has strengthened by 30% from 1994-2019. We subdivided the ODZ into a core and a deep layer based on potential density and revealed that different processes control the magnitude of fixed nitrogen loss between these regions. We postulate that the depth of the upper ETNP ODZ water mass, the 13 ºC Water, influences the organic carbon supply to the core ODZ and therefore its strength. We correlated the maximum fixed nitrogen loss in the core ODZ with a nearby sedimentary nitrogen isotope record and found that this recent increase in fixed nitrogen loss has only occurred a few times over the last 1,200 years. Using this correlation, we derived the first confidence interval for the natural variability of the maximum fixed nitrogen loss within the ETNP ODZ, which has a range of 3.3 µmol kg^{-1} (p=0.01). While the current increase is only comparable to two previous events, it is within the confidence interval for natural variability (p=0.03). The deep ODZ also strengthened from 2016-2019 by approximately 30%, but this increase occurred more rapidly than the core ODZ, and this dramatic increase was not observed over the rest of the 40 years. Climate-driven intensification could lead to unprecedented changes in the ETNP ODZ within the next decade.

Plain Language Summary

Naturally occurring ocean Oxygen Deficient Zones (ODZs) play a significant role in regulating ocean nutrient availability and ecosystem structure. Climate change is expected to strengthen these ODZs. A fifty-year time series in the world's largest ODZ revealed that it has strengthened by 30% from 1994 to 2019, and based on sedimentary records, this rapid increase has only occurred twice over the last 1200 years. Although this sedimentary record suggests there is a high but not extremely certain likelihood that climate change caused this recent intensification,

continued strengthening at these rates could lead to unprecedented changes within the next decade.

1 Introduction

Open ocean Oxygen Deficient Zones (ODZs) play a pivotal role in the global nitrogen cycle (Babbin et al., 2017; Codispoti et al., 2001; Gruber and Galloway, 2008; Lam & Kuypers, 2011), carbon cycle (Cavan et al., 2017; Devol & Hartnett, 2001), and iron cycle (Heller et al., 2017; Lam et al., 2020), as well as shaping ecosystem productivity (Gallo & Levin, 2016) and predator foraging habitat (Le Croizier et al., 2022; Stramma et al., 2012). These ODZs are expected to expand due to climate change as ocean warming elevates respiration rates, increases stratification, and lowers oxygen solubility. Subsurface deoxygenation in the tropical Pacific Ocean has already been observed (Espinoza-Morriberón et al., 2021; Stramma & Schmidtko, 2021), but the lack of time series in ODZs hinders our ability to differentiate expansion signals from natural variability (Hawkins & Sutton, 2012). The Eastern Tropical North Pacific (ETNP) ODZ is the largest of the three oceanic ODZs (Karstensen et al., 2008; Paulmier & Ruiz-Pino, 2009) and sediment core proxies indicate that its strength has fluctuated dramatically over the past thousand years (Choumiline et al., 2019; Ontiveros-Cuadras et al., 2019; Tems et al., 2016). Nevertheless, attributing ODZ intensification to anthropogenic climate change requires estimates of its natural variability.

Many previous studies analyzing ODZ variability over time focus on ODZ size (Deutsch et al., 2014; Stramma et al., 2008, 2010). Most notably, Deutsch et al. (2014) interpreted a record of sediment particulate organic nitrogen isotopes from 1850-2010 to demonstrate that the ETNP ODZ only began strengthening around 1993, before which it was weakening. Additional work with this sediment core extended this record from 160 years to 1200 years (Tems et al., 2016). In our study, we use the amount of fixed nitrogen loss as a measure of the ODZ's strength.

2 Background

2.1 Water mass circulation and anoxia within the ETNP ODZ

The source waters to the ETNP ODZ have been identified as the 13 ºC Water, Northern Equatorial Pacific Intermediate Water (NEPIW), and modified Antarctic Intermediate Water (AAIW) (Evans, Boles, et al., 2020). All these water masses enter the ODZ oxic, but remineralization within this region and lack of external oxygen supply drive them to anoxia. Since these water masses enter the ODZ at different locations and depths, their circulation within the ODZ influences the depth of the oxygen deficient layer, where anaerobic respiration dominates. The 13 ºC Water enters from the southeast via advection in the Northern Subsurface Countercurrent (Fiedler and Talley 2006). With its core at 26.2 kg m^{-3}, the 13 ºC Water is the shallowest of the ODZ water masses. The NEPIW is injected into the ODZ along its western boundary by a Tsuchiya jet from the Northern Equatorial Undercurrent centered at 26.8 kg m^{-3} (Qiu et al., 2013). We posit that the shallower introduction of oxic water in the southeast ODZ by the 13 ºC Water and the deeper introduction of oxic water in the western ODZ by the NEPIW causes the oxygen deficient layer to be deeper in the south and shallower in the north. The deepening of the ODZ to the southeast, near the Costa Rica Dome, has been recognized for some time (Codispoti & Richards, 1976).

A Regional Ocean Modeling System (ROMS) study of oxygen supply to the ETNP ODZ, agnostic of water masses, identified two primary locations of oxygen supply in the southeastern and western borders of the ETNP ODZ through particle backtracking (Margolskee et al., 2019). These particle backtracking results match the water mass entry points described by literature, and we reproduced the particle backtracking results in Fig. 1b-c to visualize these entry points. These results indicate the cumulative amount of particle entry through the western (b) and southern (c) boundaries, highlighting both the locations as well as the potential densities of water mass sources. Specifically, the 13 ºC Water enters from the south primarily at -90 ºE at 26.2-26.3 kg m^{-3}, though its entry deepens and continues west to -140 ºE, whereas the NEPIW enters from the west around 12-15 ºN at 26.8 kg m^{-3}.

We present the potential density of the oxygen deficient layer in Fig. 1a to visualize how it is shaped by water mass entry and circulation. The data for this figure originate from a high-resolution atlas of Pacific ODZs, where 15 million measurements of 1 m-resolved oxygen concentrations were analyzed for oxygen deficient conditions (Kwiecinski & Babbin, 2021). For Fig. 1a, we average the top and bottom ODZ boundaries reported in this atlas to approximate the core of the oxygen deficient layer. This figure illustrates that the core oxygen deficient layer is shallowest between 10-15 ºN, where the NEPIW enters as a hypoxic water mass, while the oxygen deficient layer is deeper to the south where the hypoxic 13 ºC Water enters.

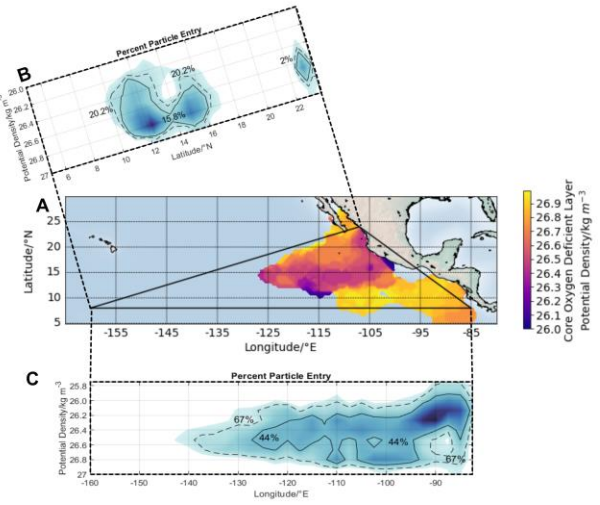

Figure 1. a) Map depicting the potential density of the oxygen deficient layer, as defined by the midpoint between the top and bottom of the ODZ, using the atlas developed by Kwiecinski & Babbin (2021). Panels (b) and (c) reproduce the results of Margolskee et al. (2019), where the sections represent the locations where water enters the ODZ on the western boundary (b) and the southern boundary (c). Percent particle entry indicates the cumulative amount of water mass-tracing particles entering the ODZ through a given boundary relative to the total, while the colormap represents the density of particle entry.

Since the 13 ºC Water and NEPIW originate and enter the ETNP ODZ from different locations, they may experience different climatic forcings. Therefore, temporal variations in ETNP ODZ anaerobic processes may vary by region due to the relative contribution of these two water masses to the oxygen deficient layer. Throughout this manuscript, we separate the ETNP

ODZ into a "core" layer between the 13 ºC Water and NEPIW (σ_θ 26.2-26.8 kg m^{-3}) and a "deep" layer between the NEPIW and the AAIW (σ_θ 26.8-27.2 kg m^{-3}). We aim for this separation to aid in identifying forcings on the temporal variability of the ETNP ODZ due to potentially different processes affecting these water masses. Notably, previous research has found that the depth of the 13 ºC isotherm and therefore the 13 ºC Water correlates with the strength of the ETNP ODZ (Deutsch et al., 2014).

The strength of the ETNP ODZ and its climatic forcings have implications beyond the ETNP ODZ itself. The 13 ºC Water and NEPIW also act as the Pacific Equatorial endmembers to the California Current System (CCS) (Evans, Boles, et al., 2020). A 40-year record of the CCS indicates that its deoxygenation correlates with the strength of the ETNP ODZ, and the NEPIW is responsible for 81% of the deoxygenation observed. (Evans, Schroeder, et al., 2020). This 50-year time series on the 110 ºW line also serves as a time series through the Pacific Equatorial endmember of the CCS, which can inform analyses of deoxygenation in the CCS.

2.2 Progression of nutrients within ETNP ODZ water masses

Water masses are defined using their temperature and salinity properties. Evans et al. (2022) filtered the World Ocean Database 2018 data for the Pacific Ocean by the temperature, salinity, and potential density of the ETNP ODZ water masses. This processing revealed the progression of nutrients in the water masses of the ETNP ODZ, depicted in Fig. 2. Analyzing the progression of nutrients within these water masses as they age reveals discrete phosphate concentrations where each water mass changes from predominantly aerobic to anaerobic respiration. These metabolic switching points are presented in Fig. 2, where the slope of NO_3^-:PO_4^{3-} switches from positive 16:1 to negative. We used these metabolic switching points as the concentrations for nutrients in the endmembers in our water mass analysis.

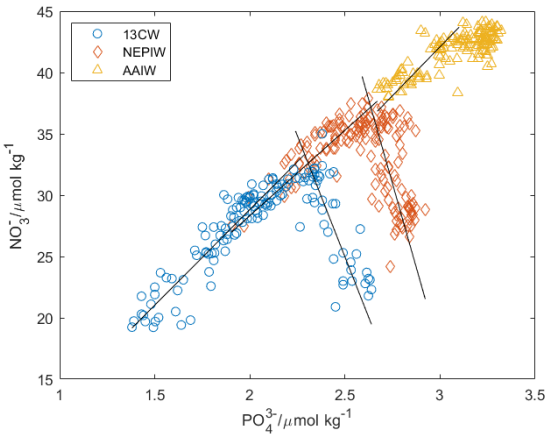

Figure 2. Progression of nutrients within the 13 ºC Water, NEPIW, and AAIW as these water masses age, with nitrate and phosphate concentrations from WOD18. Lines drawn on this figure are from Type II linear regressions. This figure is adapted from Evans et al. (2022), which provides further information about data processing for this data set.

In aerobic waters, the slope of NO_3^-:PO_4^{3-} due to respiration is close to the aerobic Redfield ratio, 16:1 NO_3^-:PO_4^{3-} due to the net nutrient stoichiometry of organic matter (Fleming 1940). The stoichiometry of organic matter consumption via nitrogen-reducing metabolisms has been calculated using the Redfield stoichiometry of organic matter as well. This reaction has a

stoichiometry of -94.4:1 NO_3^-:PO_4^{3-}, as presented in Eq. 1, and it assumes that all biological nitrogen is reduced to dinitrogen gas (Froelich et al., 1979).

$$(CH_2O)_{106}(NH_3)_{16}(H_3PO_4) + 94.4\,HNO_3 \rightarrow 106\,CO_2 + H_3PO_4 + 55.2\,N_2 + 106\,H_2O \quad (1)$$

The stoichiometry of NO_3^-:PO_4^{3-} concentrations in the water masses of the ETNP ODZ, calculated via linear regression of the anaerobic portion of each water mass in Fig. 2, differs drastically from this -94.4:1 ratio. Their stoichiometries are -39±4 and -55±6 for the 13 ºC Water and the NEPIW, respectively, due to prolific nitrite reoxidation (Evans et al., 2022).

3 Materials and Methods

3.1 Sample acquisition and measurement

The primary data for this publication were acquired on eight cruises to the ETNP between 1972-2019, seven of which transited through the center of the ETNP ODZ along the 110 ºW line. This time series spans a total of 47 years. By comparing cross-sections of the ODZ on the 110 ºW line over time, we assess the spatiotemporal variability of the ETNP ODZ. The sampling coverage provided by these cruises is highlighted in Fig. 3, which also depicts the relative frequency of observed oxygen deficient conditions sampled on the 26.5 kg m^{-3} isopycnal using the high-resolution atlas from Kwiecinski & Babbin (2021). This atlas reveals that the 110 ºW line crosses through some of the most permanently oxygen deficient waters. Data from these eight cruises have been uploaded to Zenodo (https://doi.org/10.5281/zenodo.6519188).

Temperature, salinity, oxygen, nitrate, nitrite, phosphate, and silicate were all measured with methods standardized in the U.S. Joint Global Ocean Flux Study (http://usjgofs.whoi.edu/protocols_rpt_19.html), and some of these data are presented in Fig. 4. Descriptive metadata for these cruises are contained in Table S1. Additional information about the first four cruises can be found in previous studies (Codispoti & Richards, 1976; Horak et al., 2016). Following Horak et al. (2016), we corrected for systematic errors between expeditions by applying quality control to the nitrate and phosphate data, using sigma-4 surfaces in the Global Ocean Data Analysis Project (GLODAP) Pacific data as the reference. These correction factors were applied if the offset was greater than 2% for nitrate or phosphate, and the correction factors are included in Table S2. More information about this quality control can be found in Horak et al. (2016).

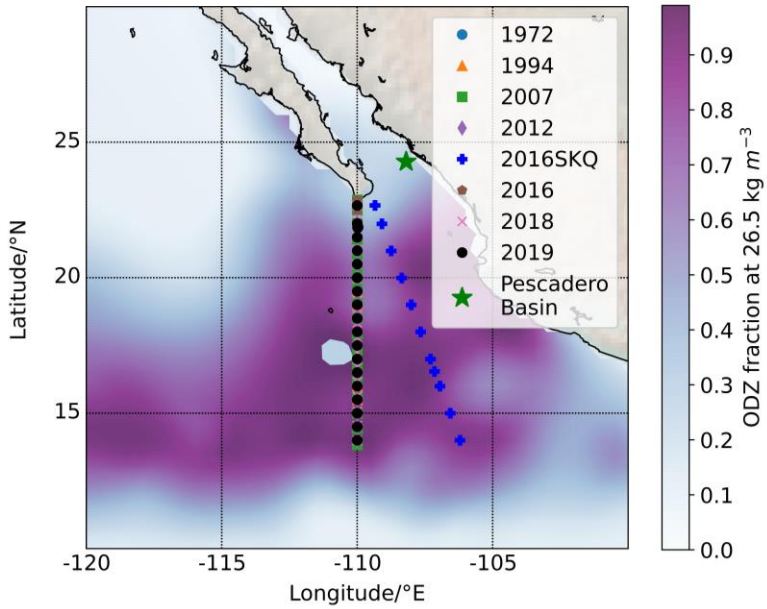

Figure 3. Map presenting the transects from the eight cruises analyzed in this study and the location of the Pescadero Basin coring site. These data are presented over a contour map of the fraction of ODZ conditions observed on the 26.5 kg m^{-3} isopycnal.

3.2 Fixed nitrogen loss via integration method

Fixed nitrogen loss was calculated using –N*, as provided in Eq. 2. In this formulation, larger –N* values indicate more fixed nitrogen has been lost and therefore the ODZ is stronger.

$$-N^* = -\left((NO_3^- + NO_2^-) - 16\,PO_4^{3-} + 2.9\right) \quad (2)$$

These –N* measurements were gridded every 0.5 degrees between 14 ºN and 23 ºN and 1 m, then integrated with a depth cumulative cubic integration routine between the integrands specified for each potential density range using MATLAB R2021A (The MathWorks, Inc. 2021). This integration approach was used in Horak et al. (2016), however, we applied different potential density ranges. Potential density ranges were selected based on the cores of water masses in the ETNP ODZ (Evans, Boles, et al., 2020), except for the shallowest density surface, 24.75 kg m^{-3}, which was used in Horak et al. (2016). The potential density of 26.2 kg m^{-3} corresponds to the 13 ºC Water (Fiedler & Talley, 2006; Qu et al., 2009), 26.8 kg m^{-3} corresponds to the potential density where the Northern Equatorial Undercurrent jets inject Northern Equatorial Pacific Intermediate Water (NEPIW) into the ETNP ODZ (Margolskee et al., 2019, Qiu et al., 2013), and 27.2 kg m^{-3} corresponds to modified Antarctic Intermediate Water (AAIW) (Bostock et al., 2013). We refer to the region between the cores of the 13 ºC Water and the NEPIW as the core ODZ because at these latitudes, oxygen is lowest and nitrite accumulates within this potential density range (Evans, Boles, et al., 2020; Larsen et al., 2016). We separate the deep ODZ into a different potential density range because typically, it is barely aerobic, though oxygen concentrations are below the detection limits for conventional sensors (Garcia-Robledo et al., 2021; Revsbech et al., 2009). We set the bottom of the ODZ at 27.2 kg m^{-3} because in this region of the ODZ, oxygen concentrations become measurable (Evans, Boles, et al., 2020). For readers interested in the depths for each of these potential density horizons, Fig.

S1 illustrates the relationship between depth and potential density. We note that N* indicates the history of fixed nitrogen loss in a water parcel, rather than the fixed nitrogen loss occurring during sample collection. Therefore, the fixed nitrogen loss we report may have occurred elsewhere and been transported to the sampling location. We estimate if the observed fixed nitrogen loss occurred primarily at the sampling location by comparing the potential density of observed fixed nitrogen loss against the potential density of the oxygen deficient layer (Fig. 1).

3.3 Fixed nitrogen loss via water mass analysis

Estimates of fixed nitrogen loss with N* often incorporate an offset value to correct for preformed nutrients. This offset value is often 2.9, which reflects the regression of nitrate and phosphate in the global ocean data set (Gruber and Sarmiento, 1997). Rather than using this globally averaged offset value, water mass analysis allows us to set an offset value specific for the mixture of water masses in the ETNP ODZ. We used the metabolic switching points between aerobic and anaerobic respiration for each ETNP water mass because this concentration is the approximate concentration where anaerobic metabolisms begin to dominate. This approach provides more accurate estimates for the nutrient offset values in the ODZ.

In our previous paper, Evans et al. (2023), we posited that N* overestimates fixed N loss due to nitrite reoxidation. Instead, it is important to remember that N* includes the loss of both dissolved inorganic nitrogen as well as particulate ammonia (Sarmiento and Gruber 1997). Therefore, N* does not overestimate fixed N loss, rather, our method calculates dissolved inorganic nitrogen loss only. To scale our fixed N loss calculated via eOMP to match N*-based estimates, they can be corrected by multiplying them by 1.16, which includes that amount of fixed nitrogen lost per phosphate equivalent, assuming the Redfield ratio of 16:1.

We used extended optimum multiparameter analysis (eOMP) for this water mass analysis. This method requires that we define endmember nutrient concentrations as well as specify a stoichiometry for fixed nitrogen loss. We grounded our fixed nitrogen loss stoichiometry in the observed stoichiometry for anaerobic remineralization in the ETNP ODZ (Fig. 2, values provided in Evans et al., 2022). With regards to the range of NO_3^-:PO_4^{3-} stoichiometries observed, we selected –62.1:1 NO_3^-:PO_4^{3-} as the stoichiometry for fixed nitrogen loss in our eOMP analysis because it had the best fit within the range of NO_3^-:PO_4^{3-} stoichiometries observed.

An additional benefit of using eOMP to calculate fixed nitrogen loss is that it lowers overestimation due to nitrite reoxidation. N* quantifies the difference between nitrate, nitrite, and phosphate concentrations, the former of which is attenuated by nitrite reoxidation. Instead, the eOMP applied here calculates the concentration of nitrate consumed along the -62.1:1 stoichiometry, which is within the range of observed stoichiometries for NO_3^-:PO_4^{3-} for anaerobic respiration in the ETNP ODZ.

Extended optimum multiparameter analysis (eOMP) calculations were performed using the GUI option in a modified version of the omp2 MATLAB package written by Johannes Karstensen and Matthias Tomczak (Karstensen, 2023), which has been uploaded to https://doi.org/10.5281/zenodo.6519316. The original version of this software can be found at https://www.mathworks.com/matlabcentral/fileexchange/1334-omp-analysis. All computations besides the integrations were performed using MATLAB R2018B (The MathWorks, Inc. 2018). The basis of water types for eOMP were selected primarily based on their endmembers in Evans

et al. (2020), except upper Pacific Subarctic Water (uPSUW). Instead, this water type was taken from the California Current System (Bograd et al., 2019). In a previous water mass analysis of the ETNP ODZ, nutrient concentrations were adjusted to the most representative values for each cruise. While this method provides robust analysis of water mass distributions, it does not calculate the fixed nitrogen loss. Conservative temperature (θ), absolute salinity (S_A), phosphate (PO_4^{3-}), nitrate (NO_3^-), silicate (SiO_4^{2-}), and potential density anomaly (σ_θ) were used as parameters for this eOMP, and the equation used to calculate the water mass content as well as fixed nitrogen loss is provided in Eq. S3. Thermodynamics Equation of State 10 (TEOS-10) was used to convert *in situ* temperature and salinity to conservative temperature and absolute salinity, as well as calculate potential density anomaly, using IBM ILOG CPLEX Optimization Studio V12.8.0 as an optimizer (McDougall & Barker, 2011). Maps were plotted using Python 3.7.13 (Python Software Foundation, 2022) in Spyder 5.1.5 (Raybaut, 2009) with the Basemap package (Hunter, 2007).

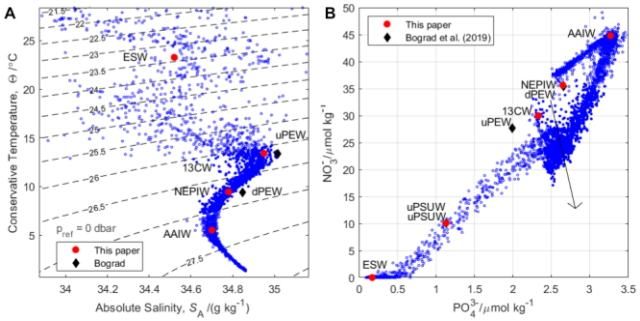

Figure 4. Data from the eight cruises in this 50-year time series in blue presented with water mass endmembers. Plots illustrate θ versus S_A (a) and NO_3^- versus PO_4^{3-} (b) where closed blue circles are samples within the potential density range that we used for eOMP analysis and open circles are other samples from these cruises. Red circles represent water mass endmembers for the ETNP ODZ, where uPSUW, 13 ºC Water, NEPIW, and AAIW were used in our eOMP analysis. The uPSUW endmember is excluded from the θ-S_A diagram because it has far lower salinity than the other endmembers. The NO_3^--PO_4^{3-} plot includes the endmembers of equivalent water masses in Bograd et al. (2019) as black diamonds to facilitate comparison between the ETNP ODZ and the CCS. The arrow depicted on this figure represents the -62.1:1 NO_3^-:PO_4^{3-} stoichiometry used for fixed nitrogen loss, and the eOMP calculation uses this stoichiometry to match the nutrient concentrations to the measured values by adjusting the nutrient values from a combination of 13 ºC Water, NEPIW, and AAIW nutrient endmembers.

Nutrient (PO_4^{3-}, NO_3^-, and SiO_4^{2-}) concentrations for the 13 ºC Water , NEPIW, and AAIW endmembers were selected by identifying the metabolic switching points for each water mass in the ETNP ODZ (Evans et al., 2022). Parameter weightings were based on Evans et al. (2020) and Evans et al. (2022). Our selected stoichiometry for fixed nitrogen loss was derived from the same data, then this stoichiometry, water mass endmembers, and weightings were refined by slight adjustments to minimize the sum of squared residuals output from the eOMP (Table S4). These adjustments were performed to ensure our parameterization of the input hydrographic parameters and nutrients accurately reproduced the measured data. The Supplemental Information contains more details about this eOMP.

3.4 Data processing for time series comparison`

Our eOMP analysis calculates the amount of fixed nitrogen loss that occurred in every sample relative to the nutrient concentration of the water masses before anaerobic processes begin to accumulate. We convert the accumulated anaerobic remineralization to NO_3^- equivalents by scaling it by 62.1, the stoichiometry we used for relating NO_3^- to PO_4^{3-}. However, one goal of this paper is to calculate the ETNP ODZ strength during this 50-year time series to facilitate comparison against other time series (Fig. 6). To quantify the strength of the core and the deep ODZ, we filtered the eOMP fixed nitrogen loss into the same potential density ranges as the integrated N*, extracted eOMP fixed nitrogen loss samples greater than or equal to the 90% quantile for each cruise, and computed the mean and standard deviation of these samples. This metric identifies water parcels with an integrated history of fixed nitrogen depletion, and we can use the extent of depletion in these parcels to quantify the total ODZ strength. The 90% quantile was selected to ensure that a single outlier did not bias the data, but the given values still represent the most intense fixed nitrogen loss sampled on each cruise. We verified that the trend in core ODZ strength is not sensitive to quantile threshold by comparing the 80%, 85%, 90%, and 95% quantiles (Fig. S6). We found that the 80%-90% quantiles have statistically equivalent trends, while the 95% quantile deviates slightly, likely because the number of samples being averaged is consistently less than or equal to five. Table S5 reports the mean, standard deviation, and number of samples for each potential density range in the 90% quantile. Throughout this paper, we refer to this metric as the "maximum fixed N loss calculated via eOMP". We report fixed N loss through this metric because it enables a more precise estimation of the nutrient concentration during the switch to anaerobic metabolisms. This metric may undergo future revisions during use in other publications and discussions in the field, however, it is a first attempt at increasing precision with regards to fixed N loss in ODZs.

Research on the California Current System has identified that its Pacific Equatorial source waters originate from a location on the 110 ºW line (Bograd et al, 2019). To generalize our time series for broader audiences, we compared the ETNP ODZ data against a record of data from the CCS collected by the California Cooperative Fisheries Initiative (CalCOFI). For the CalCOFI O_2 data presented in Fig. 2e, all samples between 100 m and 400 m for every station were averaged for every year and quarter, as performed in Evans et al. (2020). This intermediate dataset was uploaded to the same Zenodo repository for repeatability and attached as Table S6. A Grubbs test for outliers was performed for the four quarterly cruises each year, and then the mean and standard deviation was calculated for the remaining values.

Previous work has correlated the strength of the ETNP ODZ, as measured via sedimentary nitrogen isotopes, with the depth of the 13 ºC isotherm taken from the World Ocean Database (Deutsch et al., 2014). We analyzed the depth of the core of the 13 ºC Water, similar to the depth of the 13 ºC isotherm, on the eight cruises in our time series to compare against ODZ strength quantified with the maximum fixed N loss calculated via eOMP. The depth of the 13 ºC Water was calculated by converting the 1-m binned data for each cruise into conservative parameters via TEOS-10, identifying the depth of all samples where $13.31\ ºC \leq \theta \leq 13.51\ ºC$, then taking the mean and standard deviation of these samples between 14 – 19 ºN. Stations north of 19 ºN were removed because the Gulf of California leads to a confluence of water masses that creates a transition zone at these locations (Contreras-Catala et al., 2021), as well as introducing Gulf of California Water (Castro et al., 2000), which could artificially bias this calculation. The

mean, standard deviation, and number of samples for each cruise is specified in Table S7 and the depth for each station and cruise is presented in Fig. S5.

To examine whether the fixed nitrogen loss we observed was advected from elsewhere in the ODZ, we compared the locations of our observed fixed nitrogen loss against estimates of oxygen deficient layer density surfaces in the Eastern Pacific. If fixed nitrogen loss is observed outside the oxygen deficient layer, then that fixed nitrogen loss likely occurred elsewhere. We calculated the core oxygen deficient layer potential density by averaging the top and bottom potential densities of the ODZ specified in Kwiecinski & Babbin (2021), and we recreated a figure of water entry into the ODZ from Margolskee et al. (2019) with data shared by the author and contour lines added by eye (Fig, 1). The data and code for these analyses are included in the appropriate Zotero repositories for this paper.

3.5 Natural variability estimation via sediment core conversion

A primary goal in this study was to assess if modern changes in ETNP ODZ strength are unprecedented and therefore could be attributed to anthropogenic climate change with high confidence. For this analysis, we required a time series of the ETNP ODZ with enough temporal measurements to assess its natural variability. Tems et al. (2016) measured sedimentary nitrogen isotopes from the Pescadero basin that spanned nearly 1200 years, which Deutsch et al. (2014) correlated with ODZ strength. The supplemental information in Tems et al. (2016) contains the entire Pescadero basin sediment core record. The 20-point smoothing algorithm used for the data they published removed the last 10 points, which overlaps with our water column data, so we smoothed the original data with a moving boxcar approach to retain the tail of these data. We applied a length 7 boxcar and the "rloess" smoothing method in MATLAB R2018B because this smoothing algorithm best fit their data from 1970-2010. The initial data, their smoothed data, and our smoothed data are displayed in Fig. S5. We applied a linear interpolation to this smoothed data to estimate the δ^{15}N-PON at the same timepoints as the water column data and extrapolated with the same linear method from 2010 to 2012. Our converted data are presented in Fig. S5. This extrapolation allowed us to use four points, rather than three, for comparison with the Pescadero basin data. We determined a conversion from these interpolated Pescadero basin points to the maximum fixed nitrogen loss measured before 2016 using singular value decomposition (Glover et al., 2011) with the formulation in Eq. 3. These confidence intervals can be directly added to the water mass nutrient endmembers of the 13 ºC Water and NEPIW. Additional statistical information is provided in the Supplemental Information.

$$Max\ fixed\ N = m\left(\delta^{15}\mathrm{N}_{interp}\right) + b \quad (3)$$

4 Results

4.1 Fifty years of fixed nitrogen loss

ODZs are defined as oceanic regions that facilitate fixed nitrogen loss through denitrification, anammox, and other processes, due to the absence of sufficient oxygen as a terminal electron acceptor. We first examined ODZ variability by calculating the nitrogen deficit relative to phosphate concentrations using –N*, then integrating that parameter across the ODZ using a previously defined method (Horak et al., 2016). We found that the integrated fixed nitrogen loss in this cross-section of the ETNP ODZ has increased almost monotonically from 1972-2019, with slight decreases in 1994 and 2018 (Fig. 5a). The upper oxycline of the ODZ

contributes negligibly to the total fixed nitrogen loss (Fig. 5b), whereas the core ODZ and the deep ODZ share similar contributions to the total fixed nitrogen loss (Fig. 5c). The integrated fixed nitrogen loss in 2019 is 30% larger than what was measured in 1994, and this intensification was caused by an already intense core ODZ combined with a dramatic increase in deep ODZ strength, as quantified by the maximum fixed N loss calculated via eOMP after 2016 (Fig. 6a). The magnitude of this post-2016 deep ODZ intensification is not observed in the previous 40 years and may be unprecedented.

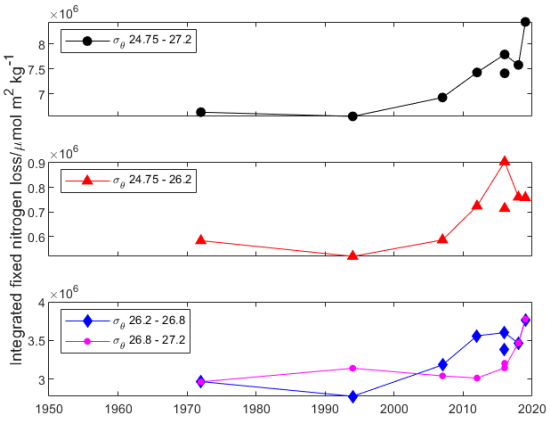

Figure 5. Integrated –N* values for each cruise, filtered between the specified potential density ranges such that (a) is the total ODZ, (b) is the upper oxycline, and (c) depicts both the core ODZ and the deep ODZ, which contains the deeper oxycline. Both 2016 cruises are presented, and SKQ201617S is the systematically low point not connected by a line on each plot, also labeled as "SKQ".

For robustness, we compared this integrated fixed nitrogen loss, calculated via –N* (Eq. 2), against the ODZ strength, quantified as the maximum fixed N loss calculated via eOMP (Eq. S2-4. The maximum fixed N loss calculated via eOMP (Fig. 6a) ranged from 9.45±0.65 to 11.85±0.35 μmol kg^{-1} in the core and 7.25±0.17 to 9.76±0.48 μmol kg^{-1} in the deep ODZ. The maximum fixed N loss calculated via eOMP correlated with the integrated fixed nitrogen loss (Fig. 5c,6a; Table 1), and cross-sections of the ODZ nitrogen loss, calculated using eOMP, over time are shown in Fig. 8).

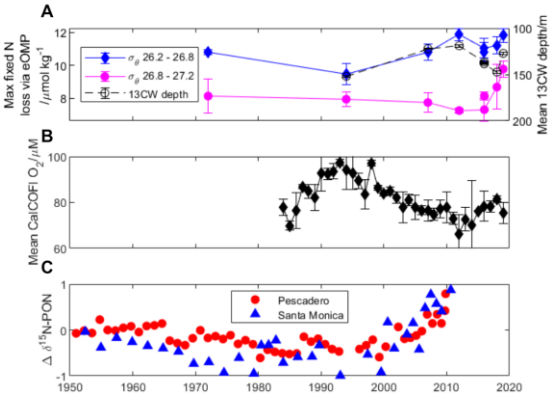

Figure 6. (a) depicts the maximum fixed N loss calculated via eOMP , reported for each cruise within the potential density ranges in the integrations in Fig. 5c. Error bars correspond to standard deviation in the maximum 10% of fixed N loss values derived via eOMP. The depth of the 13 ºC Water is plotted on the right y-axis. (b) depicts the mean oxygen concentration measured between 100-400 m on CalCOFI cruises for southern California, and error bars correspond to the seasonal standard deviation. (c) depicts normalized particulate organic nitrogen isotopes measured and published in Deutsch et al. (2014) for comparison.

Previous research suggests that water masses from the ETNP ODZ are the origin of 81% of the deoxygenation observed in the California Current System (CCS) (Evans, Schroeder, et al., 2020). The 110 ºW line studied in this 50-year time series contains the location for the Pacific Equatorial endmember of the CCS (Bograd et al., 2019; Thomson & Krassovski, 2010), and using our data, we confirm that the maximum fixed N loss calculated via eOMP of the core ETNP ODZ (Fig. 6a) correlates with the mean oxygen concentration of the southern, subsurface CCS (Fig. 6b). We also confirm that a previous record of nitrogen isotopes from sediment cores, replotted in Fig. 6c, correlate with the maximum fixed N loss calculated via eOMP in the water column (Fig. 6a). Deutsch et al. (2014) initially used this isotopic record to argue for changes in ODZ size, but since it reflects the extent of denitrifying processes, it also represents the maximum fixed nitrogen loss. Therefore, we interpreted this record of sediment nitrogen isotopes as a record of ODZ strength.

Table 1. Summary of linear correlation coefficients between time series. SKQ2016 was omitted from these calculations when relevant.

	Integrated –N*	Max fixed N loss (eOMP)	Pescadero δ^{15}N-PON	13 ºC Water depth	Mean CalCOFI O_2
Integrated –N*	1	0.842	0.980	0.503	0.744
Max fixed N loss (eOMP)	0.842	1	0.987	0.691	0.890
Pescadero δ^{15}N-PON	0.980	0.987	1	0.926	0.995
13 ºC Water depth	0.503	-0.691	-0.926	1	0.890
Mean CalCOFI O_2	0.744	-0.890	-0.995	0.890	1

4.2 Natural variability of the ETNP ODZ

Sediment nitrogen isotope records can illuminate historical trends in the strength of the core ETNP ODZ. The correlation between the maximum fixed N loss calculated via eOMP of the core ETNP ODZ and the Pescadero sediment nitrogen isotope record suggests that the core of the ODZ can be compared against this time series, but the deep ODZ cannot be. We converted the 1,200-year long Pescadero sediment core nitrogen isotope record (Tems et al., 2016) to equivalent water column data by fitting overlapping nitrogen isotope data to the maximum fixed nitrogen loss calculated via eOMP in the core ODZ, as plotted in Fig. 7a. We then extrapolated this fit to the entire isotopic record, which provides a record of core ODZ strength, quantified with the maximum fixed N loss calculated via eOMP, over the past 1,200 years. We determined the frequency distribution of this proxy for fixed nitrogen loss (Fig. 7b) and applied a 99% confidence interval to identify thresholds for virtually certain climate change forcings by the

standards of the Intergovernmental Panel on Climate Change (Mastrandrea et al., 2011) on fixed nitrogen loss in the ETNP ODZ. All our timepoints fall within the 99% confidence threshold, such that we cannot yet be virtually certain that climate change has caused the intensification of the core ETNP ODZ. The 2012 and 2019 time points both have 96% confidence thresholds, which are "very likely" to be caused by climate change but not "virtually certain".

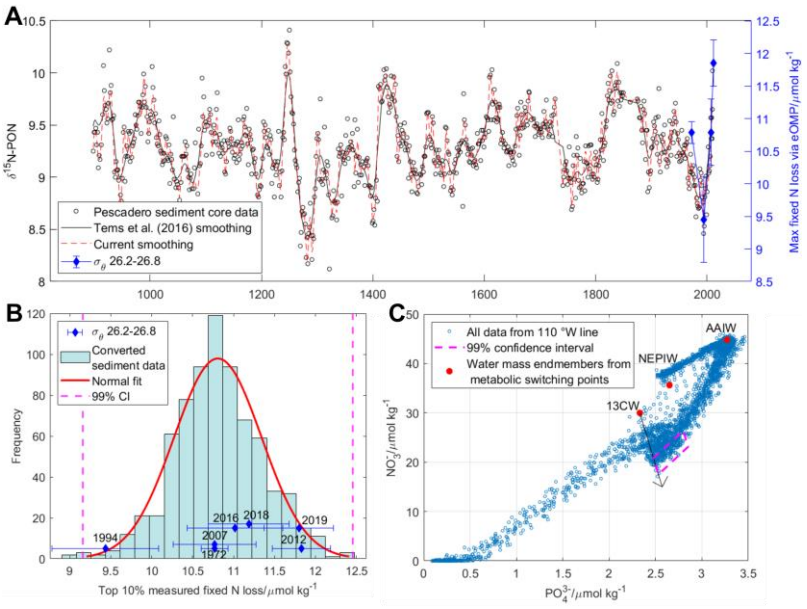

Figure 7. a) δ^{15}N-PON Pescadero core data replotted from Tems et al. (2016) with the maximum fixed N loss from the core ODZ from the relevant years overlaid as blue diamonds. b) Points depicting the maximum fixed N loss from the core ODZ and a histogram of δ^{15}N-PON Pescadero core data from Tems et al. (2016) converted to maximum fixed nitrogen loss based on the comparison in (a). This figure includes the 99% confidence intervals of this distribution in dashed magenta lines. Error bars here correspond to error bars in Fig. 6. Maximum fixed N loss points in this figure have their vertical position adjusted so they do not overlap. c) NO_3^--PO_4^{3-} plot of data from the eight cruises, where the magenta box corresponds to the 99% confidence interval determined in (a) This plot includes the water mass endmembers and the fixed N loss vector used to derive this confidence interval.

This data treatment indicates that the natural variability of maximum fixed nitrogen loss calculated via eOMP in the core ETNP ODZ on the 110 ºW line over 1,200 years has a range of 3.3 µmol kg^{-1}, corresponding to 9.2-12.5 µmol kg^{-1} of maximum fixed nitrogen loss from our reference eOMP water mass endmembers. To facilitate the use of this confidence interval by future scientists, we present it as a region on a NO_3^--PO_4^{3-} plot of ETNP ODZ data from the 110 ºW line, which removes the eOMP water mass endmember nutrient values. The upper left and lower right sides of this parallelogram represent the 99% confidence interval for the maximum fixed nitrogen loss, as plotted in Fig. 7b. Should the maximum 10% of nutrients sampled on the 110 ºW line between σ_θ 26.2-26.8 kg m^{-3} exceed the lower right side of that parallelogram, we can be virtually certain that climate change is responsible for ETNP ODZ intensification. Overall, this analysis demonstrates that the current conditions of the ETNP ODZ are near the limit of its natural variability, and it could exceed this natural variability within the next decade.

5 Discussion

Our findings reveal that the strength of the ETNP ODZ, quantified as –N* and characterized along the 110 ºW line, decreased slightly from 1972 to 1994 then nearly monotonically increased by 30% in 2019 relative to 1994. We subdivided the ODZ into the upper oxycline, the core ODZ, and the deep ODZ. We found that the core and deep ODZ contribute similarly to the integrated fixed nitrogen loss. The deep ODZ intensified significantly after 2016, which is unprecedented throughout this 50-year time series and contributes to the strongest ODZ in 2019. Using an extended optimum multiparameter analysis (eOMP), we confirmed that the maximum fixed nitrogen loss in the core ODZ correlates with sediment core nitrogen isotopes and the mean oxygen in the southern, subsurface California Current System (CCS).

Deutsch et al. (2014) also found that this sedimentary nitrogen isotope record correlated with the depth of the 13 ºC isotherm, which is a defining property of the 13 ºC Water in this region (Evans, Boles, et al., 2020). We discovered a strong correlation (p=–0.69) between the depth of this water mass and the maximum fixed N loss calculated via eOMP of the ODZ core (Fig. 6a) and an even stronger correlation (p=0.89) between the 13 ºC Water depth and the mean oxygen concentration in the southern, subsurface CCS. Since the 13 ºC Water depth sets the thermocline depth in the ETNP, we suggest that shoaling of the 13 ºC Water leads to higher organic carbon flux into the subsurface waters of the ETNP, which fuels both aerobic and anaerobic respiration, causing oxygen depletion (Fig. 6b) as well as fixed nitrogen loss (Fig. 6a). Therefore, the depth of the 13 ºC Water plays an important role on the strength of remineralization in general across the ETNP.

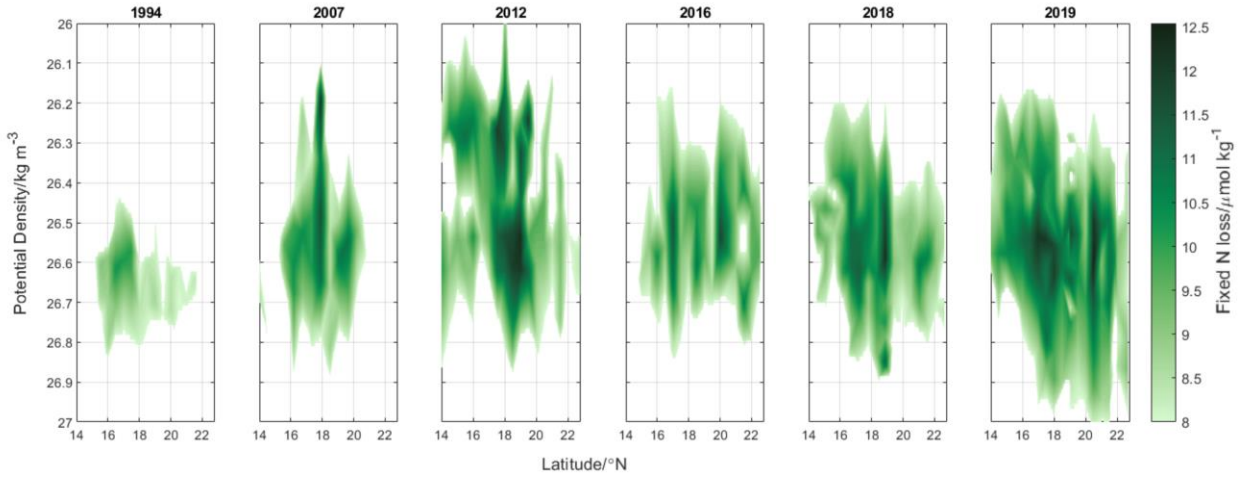

Figure 8. Cross-sections of fixed nitrogen loss as calculated with eOMP in the ODZ on the 110 ºW line for each year except 1972. As some fixed nitrogen loss occurs at every density horizon in the region, we only plotted fixed nitrogen loss greater than 8 µmol kg^{-1} to better visualize changes in the spatial coverage of fixed nitrogen loss.

The strengthening of the core ODZ (σ_θ 26.2-26.8 kg m^{-3}) presented in Figs. 5c and 6a is linked to shallowing of the ODZ, most obvious in the trend from 1994 to 2012 (Fig. 8). Deepening of the ODZ past σ_θ 26.8 kg m^{-3} is responsible for the rapid intensification in the deep ODZ observed in 2018 and 2019. This deepening does not follow the same temporal trend as the shallowing of the core ODZ, suggesting that these processes have different causes.

The locations of ODZ intensification during this time series differ for the core versus the deep ODZ (Fig. 8). In 2007, 2012, and 2019, the core ODZ is stronger at and south of 18 ºN, whereas in 2018 and 2019, the deep ODZ is stronger at and north of 18 ºN. Comparing these locations against the 110 ºW line on Fig. 1a, the oxygen deficient layer is centered around 26.7 kg m^{-3} at 18 ºN and deepens further north, closer to Baja. This distribution of the oxygen deficient layer matches the strengthening of the ODZ (Fig. 8). Therefore, we propose that the intensification of the core ODZ occurred between 14-18 ºN whereas the intensification of the deep ODZ occurred between 18-22 ºN. This conclusion is notable because the results deviate from the conventional trend that a deeper oxygen deficient layer occurs farther south in the ETNP, and thus the fixed nitrogen loss we observed likely occurred in the north.

Our comparison between sedimentary nitrogen isotopes and water column fixed nitrogen loss calculated via eOMP demonstrates that we cannot yet be virtually certain that climate change has caused core ODZ intensification. Only two events around 1230 and 1400 CE possessed the rapid strengthening observed in the past 30 years, and both events were followed by ODZ weakening. It remains to be seen if the current event will follow this pattern, and should the core ODZ strength continue increasing, it will exceed historical precedent within the next decade. While this analysis relies on only four timepoints, it provides a first estimate at the natural variability of fixed nitrogen loss in the ETNP ODZ. More recent sediment data could extend this comparison from four to seven points, and in the supplemental information we include the data and code needed to improve our calculations should this more recent sediment core data become available. Fig. 7c depicts the region of natural variability in NO_3^--PO_4^{3-} space for reference, and these values are also included in the Supplemental Information.

Our analysis of natural variability focused only on the core ODZ and did not include the deep ODZ, which also became 30% stronger from 2016 to 2019. A sediment core from a location that records processes in the deep ODZ would be useful to address this topic through a similar analysis. While the primary forcing on fixed nitrogen loss in the core ODZ appears to be the shoaling of the 13 ºC Water, caused by trade wind stress on basin-wide scale, the authors are not aware of the primary forcings for the deep ODZ that caused its rapid intensification. Nevertheless, we hypothesize that the primary forcing is linked to the NEPIW. Oxygen deficient conditions in the deep ODZ are influenced by the NEPIW, which governs how far north the deep ODZ extends. The NEPIW is formed by subsurface mixing of Pacific Deep Water and Antarctic Intermediate Water, with some North Pacific Intermediate Water. The North Pacific Intermediate Water and the upper part of the Pacific Deep Water experienced between -0.68 to -0.39 µmol kg^{-1} $year^{-1}$ of deoxygenation from 1956-2006 (Whitney et al., 2007), and if the oxygen supply to the NEPIW lowered, anoxia would occur earlier and therefore more fixed nitrogen loss would occur. We recommend further analysis of climatic forcing of the deep ODZ, likely through the NEPIW, be performed to better understand nitrogen cycling in the Pacific Ocean.

Though we lack the natural variability of the deep ODZ, our estimate of the natural variability of the core ODZ can still inform projections of ODZ strength and size. We focus on fixed nitrogen loss rather than oxygen concentration because conventional sensors struggle to differentiate low oxygen and oxygen deficient conditions, which impedes statistical comparisons. In addition, we focus on ODZ intensification rather than ODZ expansion for two reasons. First, the cross-sections our study relies on cannot accurately capture ODZ volume. In addition, mesoscale features such as eddies spread and distribute ODZ water outside of its traditional bounds (Evans, Boles, et al., 2020; Resplandy et al., 2011) as well as inject non-ODZ water into

its domain (Margolskee et al., 2019), hindering the ability of discreet sampling to quantify the size of an ODZ.

6 Conclusions

Intensification of Oxygen Deficient Zones is a globally relevant issue due to their significant role in biogeochemical cycling and influence on ecosystem biogeography. Prokaryotic metabolisms drive most of biogeochemical cycling in ODZ regions. These metabolisms employ electron donors and acceptors other than carbon and oxygen such as trace metals, sulfur, and particularly nitrogen via N_2 gas production as well as N_2O cycling. N_2O is a potent greenhouse gas, while N_2 production influences the marine fixed nitrogen inventory. In vast areas of the ocean, the availability of fixed nitrogen limits primary production, and the balance between N_2 fixation and production regulates this inventory. A strengthening ODZ could result in increased denitrification, lowered primary production, and therefore a diminished biological carbon pump.

This 50-year time series is, to the best of our knowledge, the longest time series from the water column of an ODZ in scientific literature, and it provides valuable insight into changes that have occurred within the ETNP ODZ. Most importantly, we generated a first estimate for the natural variability of this ODZ. This result indicates that the core ODZ has only been this strong twice in the past 1,200 years, but we cannot yet attribute this recent ODZ intensification to climate change. The IPCC defines their threshold as p=0.01 (Mastrandrea et al., 2011), and our data remains at p=0.03. Nevertheless, our distribution of the historical fixed nitrogen loss in the ETNP ODZ can be used to refine simulations of ETNP ODZ processes and to identify important differences in processes that influence the deep versus the core ODZ. The correlation between the 13 ºC Water mass and the strength of the ETNP ODZ, quantified with the maximum fixed N loss calculated via eOMP, reveals that the 13 ºC Water significantly impacts ETNP processes. Due to the correlation and slight lag between the depth of the 13 ºC Water mass in the ETNP and the amount of deoxygenation in the southern CCS, we suggest that real time monitoring of the 13 ºC Water depth in the ETNP ODZ, potentially with Argo floats, could forecast deoxygenation in the CCS. This monitoring, as well as confidence intervals for natural variability, are crucial for future oceanographers and geoscientists as we monitor, forecast, and respond to climate change and its consequences on ocean biogeochemistry, ecosystem health, and fishery production.

Acknowledgments

Sampling cruises on the 110 ºW line were funded by NSF OCE-1636332, DEB-1542240, OCE-1046017, OCE-1029951, and OCE-1657958. NE was funded by OCE-2023708 during the processing and writing of this manuscript. JT was funded to work on this project by a fellowship through the University of Southern California Wrigley Institute for Environmental Studies. We greatly appreciate the efforts required in funding, coordinating, and measuring data in the WOCE, CLIVAR, and CalCOFI programs, as well as the work required to create consensus

nutrient concentrations in the GLODAP program and the effort that went into acquiring these extensive sediment core records. We thank Mattias Tomczak and Joseph Karstensen for writing the MATLAB omp2 package used for conducting this water mass analysis, as well as David Glover, William Jenkins, and Scott Doney for documenting several statistical techniques used in this analysis in their book Modeling Methods for Marine Science. We would like to acknowledge Isaac Schroeder for sharing CalCOFI data updated to 2019, as compared to data circa 2018 as used in Evans et al. (2020). We would like to acknowledge Caitlin Tems for sharing the Pescadero and Santa Monica basin particulate organic nitrogen isotope core record data.

Open Research

The data products used in this analysis are stored in Zenodo at https://doi.org/10.5281/zenodo.6519188, and the code used in this analysis is stored at in Zenodo at https://doi.org/10.5281/zenodo.6519316. All code is well-commented to facilitate future use and the data products that are specifically plotted in this paper are saved as separate, labeled files for convenience. In addition to these repositories, the CalCOFI dataset can be found at www.calcofi.org. While the MATLAB code for the water mass analysis and the TEOS-10 conversions were acquired at https://www.mathworks.com/matlabcentral/fileexchange/1334-omp-analysis and http://www.teos-10.org/, appropriately, they have also been uploaded to the same Zenodo repository to enable other researchers.

The authors declare no conflicts of interest.

References

Babbin, A. R., Peters, B. D., Mordy, C. W., Widner, B., Casciotti, K. L., & Ward, B. B. (2017). Multiple metabolisms constrain the anaerobic nitrite budget in the Eastern Tropical South Pacific: Nitrogen Dynamics in the Eastern Tropical South Pacific. *Global Biogeochemical Cycles*. https://doi.org/10.1002/2016GB005407

Bograd, S. J., Schroeder, I. D., & Jacox, M. G. (2019). A water mass history of the Southern California current system. *Geophysical Research Letters*, *46*(12), 6690–6698. https://doi.org/10.1029/2019GL082685

Bostock, H. C., Sutton, P. J., Williams, M. J. M., & Opdyke, B. N. (2013). Reviewing the circulation and mixing of Antarctic Intermediate Water in the South Pacific using evidence from geochemical tracers and Argo float trajectories. *Deep Sea Research Part I: Oceanographic Research Papers*, *73*, 84–98. https://doi.org/10.1016/j.dsr.2012.11.007

Castro, R., Mascarenhas, A. S., Durazo, R., & Collins, C. A. (2000). Seasonal variation of the temperature and salinity at the entrance to the Gulf of California, Mexico. *Ciencias Marinas*, *26*(4), 561–583. https://doi.org/10.7773/cm.v26i4.621

Cavan, E. L., Trimmer, M., Shelley, F., & Sanders, R. (2017). Remineralization of particulate organic carbon in an ocean oxygen minimum zone. *Nature Communications*, *8*(1), 1–9. https://doi.org/10.1038/ncomms14847

Choumiline, K., Pérez-Cruz, L., Gray, A. B., Bates, S. M., & Lyons, T. W. (2019). Scenarios of Deoxygenation of the Eastern Tropical North Pacific During the Past Millennium as a Window Into the Future of Oxygen Minimum Zones. *Frontiers in Earth Science*, *7*. Retrieved from https://www.frontiersin.org/article/10.3389/feart.2019.00237

Codispoti, LA. J.A. Brandes, J.P. Christensen, A.H. Devol, S.W.A. Naqvi, H.W. Pearl and T. Yoshinari. 2001. The Oceanic fixed ntirogen and nitrous oxide budgets: moving targets as we enter the anthropocene? Sci. Mar. 65 (Suppl. 2):85-105.

612 Codispoti, L. A., & Richards, F. A. (1976). An analysis of the horizontal regime of denitrification in the
613 eastern tropical North Pacific1: Horizontal denitrification regime. *Limnology and*
614 *Oceanography*, *21*(3), 379–388. https://doi.org/10.4319/lo.1976.21.3.0379
615 Contreras-Catala, F., Beier, E. J., Sánchez-Velasco, L., Godínez, V. M., Sánchez-Pérez, E. D., &
616 Barton, E. D. (2021). Water masses and larval fish habitats in the Pacific tropical-subtropical
617 convergence off Mexico. *Continental Shelf Research*, *230*, 104575.
618 https://doi.org/10.1016/j.csr.2021.104575
619 Deutsch, C., Berelson, W., Thunell, R., Weber, T., Tems, C., McManus, J., et al. (2014). Centennial
620 changes in North Pacific anoxia linked to tropical trade winds. *Science*, *345*(6197), 665–668.
621 https://doi.org/10.1126/science.1252332
622 Devol, A. H., & Hartnett, H. E. (2001). Role of the oxygen-deficient zone in transfer of organic carbon
623 to the deep ocean. *Limnology and Oceanography*, *46*(7), 1684–1690.
624 https://doi.org/10.4319/lo.2001.46.7.1684
625 Espinoza-Morriberón, D., Echevin, V., Gutiérrez, D., Tam, J., Graco, M., Ledesma, J., & Colas, F.
626 (2021). Evidences and drivers of ocean deoxygenation off Peru over recent past decades.
627 *Scientific Reports*, *11*(1), 20292. https://doi.org/10.1038/s41598-021-99876-8
628 Evans, N., Schroeder, I. D., Pozo Buil, M., Jacox, M. G., & Bograd, S. J. (2020). Drivers of
629 Subsurface Deoxygenation in the Southern California Current System. *Geophysical*
630 *Research Letters*, *47*(21), e2020GL089274. https://doi.org/10.1029/2020GL089274
631 Evans, N., Boles, E., Kwiecinski, J. V., Mullen, S., Wolf, M., Devol, A. H., et al. (2020). The role of
632 water masses in shaping the distribution of redox active compounds in the Eastern Tropical
633 North Pacific oxygen deficient zone and influencing low oxygen concentrations in the eastern
634 Pacific Ocean. *Limnology and Oceanography*, *65*(8), 1688–1705.
635 https://doi.org/10.1002/lno.11412
636 Evans, N., Tichota, J., Moffett, J., & Devol, A. (2022, March 5). Prolific nitrite re-oxidation across the
637 Eastern Tropical North Pacific Ocean [preprint]. https://doi.org/10.1002/essoar.10511252.1

Evans, N., Tichota, J., Ruef, W., Moffett, J. W., & Devol, A. H. (2022). ETNP_ODZ_time_series [Data set]. Zenodo. https://doi.org/10.5281/zenodo.6519188

Evans, N., Tichota, J., Ruef, W., Moffett, J. W., & Devol, A. H. (2022, May 5). ETNP_ODZ_time_series_code. [Software]. Zenodo. https://doi.org/10.5281/zenodo.6519316

Fiedler, P. C., & Talley, L. D. (2006). Hydrography of the eastern tropical Pacific: A review. *Progress in Oceanography*, *69*(2), 143–180. https://doi.org/10.1016/j.pocean.2006.03.008

Fleming, R. H. (1940). Composition of plankton and units for reporting populations and production. *Proceedings 6th Pacific Science Congress*, *3*, 535–540.

Froelich, P. N., Klinkhammer, G. P., Bender, M. L., Luedtke, N. A., Heath, G. R., Cullen, D., et al. (1979). Early oxidation of organic matter in pelagic sediments of the eastern equatorial Atlantic: suboxic diagenesis. *Geochimica et Cosmochimica Acta*, *43*(7), 1075–1090. https://doi.org/10.1016/0016-7037(79)90095-4

Gallo, N. D., & Levin, L. A. (2016). Fish Ecology and Evolution in the World's Oxygen Minimum Zones and Implications of Ocean Deoxygenation. In *Advances in Marine Biology* (Vol. 74, pp. 117–198). Elsevier. Retrieved from http://linkinghub.elsevier.com/retrieve/pii/S0065288116300013

Garcia-Robledo, E., Paulmier, A., Borisov, S. M., & Revsbech, N. P. (n.d.). Sampling in low oxygen aquatic environments: The deviation from anoxic conditions. *Limnology and Oceanography: Methods*, *n/a*(n/a). https://doi.org/10.1002/lom3.10457

Glover, D. M., Jenkins, W. J., & Doney, S. C. (2011). *Modeling Methods for Marine Science*. Cambridge University Press.

Gruber N. and Galloway J.N. 2008. An earth-system perspective of the global nitrogen cycle. Nature doi:10.1038/nature06592.

Gruber, N., & Sarmiento, J. L. (1997). Global patterns of marine nitrogen fixation and denitrification. *Global Biogeochemical Cycles*, *11*(2), 235–266. https://doi.org/10.1029/97GB00077

Hawkins, E., & Sutton, R. (2012). Time of emergence of climate signals. *Geophysical Research Letters*, *39*(1). https://doi.org/10.1029/2011GL050087

Heller, M. I., Lam, P. J., Moffett, J. W., Till, C. P., Lee, J.-M., Toner, B. M., & Marcus, M. A. (2017). Accumulation of Fe oxyhydroxides in the Peruvian oxygen deficient zone implies non-oxygen dependent Fe oxidation. *Geochimica et Cosmochimica Acta*, *211*, 174–193. https://doi.org/10.1016/j.gca.2017.05.019

Horak, R. E. A., Ruef, W., Ward, B. B., & Devol, A. H. (2016). Expansion of denitrification and anoxia in the eastern tropical North Pacific from 1972 to 2012. *Geophysical Research Letters*, *43*(10), 5252–5260. https://doi.org/10.1002/2016GL068871

Hunter, J. D. 2007. Matplotlib: A 2D Graphics Environment. Computing in Science & Engineering **9**: 90–95. doi:10.1109/MCSE.2007.55

Karstensen, J. (2023). OMP Analysis (https://www.mathworks.com/matlabcentral/fileexchange/1334-omp-analysis), MATLAB Central File Exchange. [Software]. Retrieved May 27, 2023.

Karstensen, J., Stramma, L., & Visbeck, M. (2008). Oxygen minimum zones in the eastern tropical Atlantic and Pacific oceans. *Progress in Oceanography*, *77*(4), 331–350. https://doi.org/10.1016/j.pocean.2007.05.009

Kwiecinski, J. V., & Babbin, A. R. (2021). A High-Resolution Atlas of the Eastern Tropical Pacific Oxygen Deficient Zones. *Global Biogeochemical Cycles*, *35*(12), e2021GB007001. https://doi.org/10.1029/2021GB007001

Lam, P., & Kuypers, M. M. M. (2011). Microbial Nitrogen Cycling Processes in Oxygen Minimum Zones. *Annual Review of Marine Science*, *3*(1), 317–345. https://doi.org/10.1146/annurev-marine-120709-142814

Lam, P. J., Heller, M. I., Lerner, P. E., Moffett, J. W., & Buck, K. N. (2020). Unexpected Source and Transport of Iron from the Deep Peru Margin. *ACS Earth and Space Chemistry*, *4*(7), 977–992. https://doi.org/10.1021/acsearthspacechem.0c00066

Larsen, M., Lehner, P., Borisov, S. M., Klimant, I., Fischer, J. P., Stewart, F. J., et al. (2016). In situ quantification of ultra-low O2 concentrations in oxygen minimum zones: Application of novel optodes. *Limnology and Oceanography: Methods*, *14*(12), 784–800. https://doi.org/10.1002/lom3.10126

Le Croizier, G., Sonke, J. E., Lorrain, A., Serre, S., Besnard, L., Schaal, G., et al. (2022). Mercury stable isotopes suggest reduced foraging depth in oxygen minimum zones for blue sharks. *Marine Pollution Bulletin*, *181*, 113892. https://doi.org/10.1016/j.marpolbul.2022.113892

Margolskee, A., Frenzel, H., Emerson, S., & Deutsch, C. (2019). Ventilation Pathways for the North Pacific Oxygen Deficient Zone. *Global Biogeochemical Cycles*, *33*(7), 875–890. https://doi.org/10.1029/2018GB006149

Mastrandrea, M. D., Mach, K. J., Plattner, G.-K., Edenhofer, O., Stocker, T. F., Field, C. B., et al. (2011). The IPCC AR5 guidance note on consistent treatment of uncertainties: a common approach across the working groups. *Climatic Change*, *108*(4), 675–691. https://doi.org/10.1007/s10584-011-0178-6

The MathWorks, Inc. (2021). *MATLAB Release 2021a*. Natick, MA. [Software]. Retrieved from https://www.mathworks.com/products/matlab.html

The MathWorks, Inc. (2018). *MATLAB Release 2018b*. Natick, MA. [Software]. Retrieved from https://www.mathworks.com/products/matlab.html

Ontiveros-Cuadras, J. F., Thunell, R., Ruiz-Fernández, A. C., Benitez-Nelson, C., Machain-Castillo, M. L., Tappa, E., & Sanchez-Cabeza, J.-A. (2019). Centennial OMZ changes in the NW Mexican Margin from geochemical and foraminiferal sedimentary records. *Continental Shelf Research*, *176*, 64–75. https://doi.org/10.1016/j.csr.2019.02.009

Paulmier, A., & Ruiz-Pino, D. (2009). Oxygen minimum zones (OMZs) in the modern ocean. *Progress in Oceanography*, *80*(3), 113–128. https://doi.org/10.1016/j.pocean.2008.08.001

Python Software Foundation. (2022). Python Language Reference, 3.7.13 Documentation. [Software]. https://docs.python.org/release/3.7.13/

Qiu, B., Rudnick, D. L., Chen, S., & Kashino, Y. (2013). Quasi-stationary North Equatorial Undercurrent jets across the tropical North Pacific Ocean. *Geophysical Research Letters*, *40*(10), 2183–2187. https://doi.org/10.1002/grl.50394

Qu, T., Gao, S., Fukumori, I., Fine, R. A., & Lindstrom, E. J. (2009). Origin and Pathway of Equatorial 13°C Water in the Pacific Identified by a Simulated Passive Tracer and Its Adjoint.

Journal of Physical Oceanography, *39*(8), 1836–1853. https://doi.org/10.1175/2009JPO4045.1

Resplandy, L., Lévy, M., Madec, G., Pous, S., Aumont, O., & Kumar, D. (2011). Contribution of mesoscale processes to nutrient budgets in the Arabian Sea. *Journal of Geophysical Research: Oceans*, *116*(C11). https://doi.org/10.1029/2011JC007006

Revsbech, N. P., Larsen, L. H., Gundersen, J., Dalsgaard, T., Ulloa, O., & Thamdrup, B. (2009). Determination of ultra-low oxygen concentrations in oxygen minimum zones by the STOX sensor. *Limnology and Oceanography: Methods*, *7*(5), 371–381. https://doi.org/10.4319/lom.2009.7.371

Stramma, L., & Schmidtko, S. (2021). Tropical deoxygenation sites revisited to investigate oxygen and nutrient trends. *Ocean Science*, *17*(3), 833–847. https://doi.org/10.5194/os-17-833-2021

Stramma, L., Johnson, G. C., Sprintall, J., & Mohrholz, V. (2008). Expanding Oxygen-Minimum Zones in the Tropical Oceans. *Science*, *320*(5876), 655–658. https://doi.org/10.1126/science.1153847

Stramma, L., Schmidtko, S., Levin, L. A., & Johnson, G. C. (2010). Ocean oxygen minima expansions and their biological impacts. *Deep Sea Research Part I: Oceanographic Research Papers*, *57*(4), 587–595. https://doi.org/10.1016/j.dsr.2010.01.005

Stramma, L., Prince, E. D., Schmidtko, S., Luo, J., Hoolihan, J. P., Visbeck, M., et al. (2012). Expansion of oxygen minimum zones may reduce available habitat for tropical pelagic fishes. *Nature Climate Change*, *2*(1), 33–37. https://doi.org/10.1038/nclimate1304

T. J. McDougall, & Barker, P. M. (2011). *Getting started with TEOS-10 and the Gibbs Seawater (GSW) Oceanographic Toolbox*. SCOR/IAPSO WG127.

Tems, C. E., Berelson, W. M., Thunell, R., Tappa, E., Xu, X., Khider, D., et al. (2016). Decadal to centennial fluctuations in the intensity of the eastern tropical North Pacific oxygen minimum zone during the last 1200 years. *Paleoceanography*, *31*(8), 1138–1151. https://doi.org/10.1002/2015PA002904

Thomson, R. E., & Krassovski, M. V. (2010). Poleward reach of the California Undercurrent extension. *Journal of Geophysical Research: Oceans*, *115*(C9). https://doi.org/10.1029/2010JC006280

Whitney, F. A., Freeland, H. J., & Robert, M. (2007). Persistently declining oxygen levels in the interior waters of the eastern subarctic Pacific. *Progress in Oceanography*, *75*(2), 179–199. https://doi.org/10.1016/j.pocean.2007.08.007

Global Biogeochemical Cycles

Supporting Information for

Rapid expansion of fixed nitrogen deficit in the eastern Pacific Ocean revealed by 50-year time series

Natalya Evans[1], Juliana Tichota[1], Wendi Ruef[2], James Moffett[1], and Allan Devol[2]*

[1]Department of Biological Sciences, University of Southern California; Los Angeles, California.

[2]School of Oceanography, University of Washington; Seattle, Washington.

Contents of this file

Introduction

Additional information about the methods used for integration, water mass analysis, time series comparison, and natural variability estimation are provided in this document. Additional figures and tables provide visualizations and additional statistical information supporting the methods described in the manuscript as well as this Supplemental Information.

Text S1. Water mass analysis

Conservative temperature and absolute salinity were used rather than *in situ* measurements because they are more conservative across wider areas, such as on the shelf (Evans, Boles, et al., 2020). Oxygen was not used in this eOMP because within the ODZ, oxygen concentrations are below the detection limit of conventional instrumentation, such as SBE43 sensors (Revsbech et al., 2009), and report wide-ranging concentrations. Therefore, oxygen cannot be implemented in the ETNP ODZ to compare between cruises, which was a primary goal for this project. SiO_4^{2-} was included in this paper but not Evans et al. (2020) due to data availability. Evans et al. (2020) also used spiciness as a proxy for dissolved oxygen because these two parameters are hydrographically correlated in the California Current System. As Evans et al. (2020) established that these water masses are coherent on potential density surfaces and oxygen was not used in this eOMP, potential density replaced spiciness. Potential density has previously been used in other OMPs (Jenkins et al., 2015). Due to the recent development of a Python optimum multiparameter analysis package that allows for flexible constraints and underconstrained solutions (Shrikumar et al., 2022), we recommend that future scientists performing water mass analysis use this package rather than the MATLAB omp2 package, and we may also use it to re-process this data ourselves. Slight differences in the endmembers in eOMP for the ETNP ODZ on the 110 ºW exist between our formulation in the Matlab omp2 package and the pyompa package due to the addition of multiple, flexible respiration pathways in pyompa.

After the ideal eOMP settings were selected, eOMP was performed on each cruise individually with the same basis to prevent any outliers in the data from one cruise from influencing another. This step was performed because the eOMP calculation standardizes the input data. We applied eOMP between potential densities of 24.75 kg m^{-3} to 27.2 kg m^{-3} to match the integrations, however, our basis set was built for 26 kg m^{-3} to 27 kg m^{-3} to limit the inclusion of thermocline water masses in the eOMP. Our results converge best within 26 kg m^{-3} to 27 kg m^{-3}, and we caution users from using the results outside this range without scrutiny.

In most eOMP calculations, ΔP represents aerobic remineralization processes (Karstensen & Tomczak, 1998). To prevent confusion, we use ξ to represent the accumulated anaerobic remineralization. This choice of symbol is partially motivated because ξ is canonically used to represent the extent of reaction in physical chemistry(Ontiveros-Cuadras et al., 2019). This mathematics representing the use of ξ are presented in Eq. 1. The water type definitions used for quantifying water mass content are presented in Table S4. The eOMP package developed by Karstensen and Tomczak solves a linear system of equations for every sample. This system of equations is represented in general in Eq. 2, where A is the water types, x is the water mass content being solved for, and b is the measured data. Eq. 3 provides a more detailed depiction of how this paper calculated water mass content, including the residuals for each fit. Within the eOMP calculation, each parameter in Eq. 4 is standardized then weighted, but this step is not presented below for clarity. eOMP-derived fixed nitrogen loss was calculated

by multiplying ξ by 62, and the maximum fixed nitrogen loss was calculated by taking the mean of values greater than the 90% quantile for fixed nitrogen loss for each cruise. The difference between N* and 62ξ is presented in Fig. S3. For researchers interested in the relationships between these calculations, we fit N* to 62ξ using a Type 2 linear regression for values within potential densities of 26.2 kg m^{-3} to 26.8 kg m^{-3} and display the results in Eq. 4.

$$[PO_4^{3-}] = [PO_4^{3-}]_o + \xi \quad (1)$$

$$Ax - b = 0 \quad (2)$$

$$\begin{bmatrix} \theta_{ESW} & \theta_{13CW} & \theta_{NEPIW} & \theta_{AAIW} & \theta_{uPSUW} & 0 \\ S_{A,ESW} & S_{A,13CW} & S_{A,NEPIW} & S_{A,AAIW} & S_{A,uPSUW} & 0 \\ [PO_4]_{ESW} & [PO_4]_{13CW} & [PO_4]_{NEPIW} & [PO_4]_{AAIW} & [PO_4]_{uPSUW} & 1 \\ [NO_3]_{ESW} & [NO_3]_{13CW} & [NO_3]_{NEPIW} & [NO_3]_{AAIW} & [NO_3]_{uPSUW} & -62 \\ [SiO_4]_{ESW} & [SiO_4]_{13CW} & [SiO_4]_{NEPIW} & [SiO_4]_{AAIW} & [SiO_4]_{uPSUW} & 11.4 \\ \sigma_{\theta,ESW} & \sigma_{\theta,13CW} & \sigma_{\theta,NEPIW} & \sigma_{\theta,AAIW} & \sigma_{\theta,uPSUW} & 0 \end{bmatrix} \begin{bmatrix} x_{ESW} \\ x_{13CW} \\ x_{NEPIW} \\ x_{AAIW} \\ x_{uPSUW} \\ \xi \end{bmatrix} - \begin{bmatrix} \theta_{obs} \\ S_{A,obs} \\ [PO_4]_{obs} \\ [NO_3]_{obs} \\ [SiO_4]_{obs} \\ \sigma_{\theta,obs} \end{bmatrix} = \begin{bmatrix} \varepsilon_\theta \\ \varepsilon_{S_A} \\ \varepsilon_{PO_4} \\ \varepsilon_{NO_3} \\ \varepsilon_{SiO_4} \\ \varepsilon_{\sigma_\theta} \end{bmatrix} \quad (3)$$

$$62\xi = (0.883 \pm 0.026)N^* - (3.82 \pm 0.11) \quad (4)$$

We plotted the Bograd et al. (2019) Pacific Equatorial Water definitions as a helpful comparison for analyzing water masses in the eastern Pacific. uPEW and dPEW are synonymous with 13CW and NEPIW, appropriately (Evans, Schroeder, et al., 2020), but Bograd et al. (2019) defined their PEW water masses more to the southwest than the repeat hydrographic line this study focused on. In the ETNP below the thermocline, salinity slightly increases with eastward transit, as observed in longitudinal transects through the ETNP ODZ (Evans, Boles, et al., 2020). Therefore, the small shift in absolute salinity between the 13CW and NEPIW versus the uPEW and dPEW is not surprising, and it appears larger when plotted using practical salinity. The 13CW and uPEW are offset on the NO_3^--PO_4^{3-} plot, suggesting that noticeable aerobic remineralization occurs between where Bograd et al. (2019) defines their PEW water types and this sample location. This deviation fits the flow path of these water masses based on where they enter the ETNP ODZ and the remineralization that occurs as they transit (Evans et al., 2022). In the SiO_4^{2-}-PO_4^{3-} plot, the 13CW, NEPIW, and uPSUW water mass definition SiO_4^{2-}values are lowered to minimize residuals of fit.

Year	R/V	Start month	Cruise ID
1972	*Thomas G. Thompson*	February	TGT66
1994	*Discoverer*	January	WOCE_P18
2007	*Ronald Brown*	December	P18_2007
2012	*Thomas G. Thompson*	March	TN278
2016	*Ron Brown*	November	P18_2016
2016	*Sikuliaq*	December	SKQ201617S
2018	*Roger Revelle*	March	RR1804
2019	*Kilo Moana*	September	KM1919

Table S1. Table listing each cruise and metadata about each cruise.

Cruise ID	NO_3^-/µmol kg^{-1}	PO_4^{3-}/µmol kg^{-1}
TGT66	1.006	1.043
WOCE_P18	0.999	0.998
P18_2007	1.009	0.992
TN278	1.014	**1.042**
P18_2016	1.009	1.013
SKQ201617S	**1.025**	**1.082**
RR1804	**1.056**	1.004
KM1919	**1.073**	1.019

Table S2. Table containing the GLODAP corrections for each cruise, where bolded values were applied as scaling factors to correct for systemic differences in measurement.

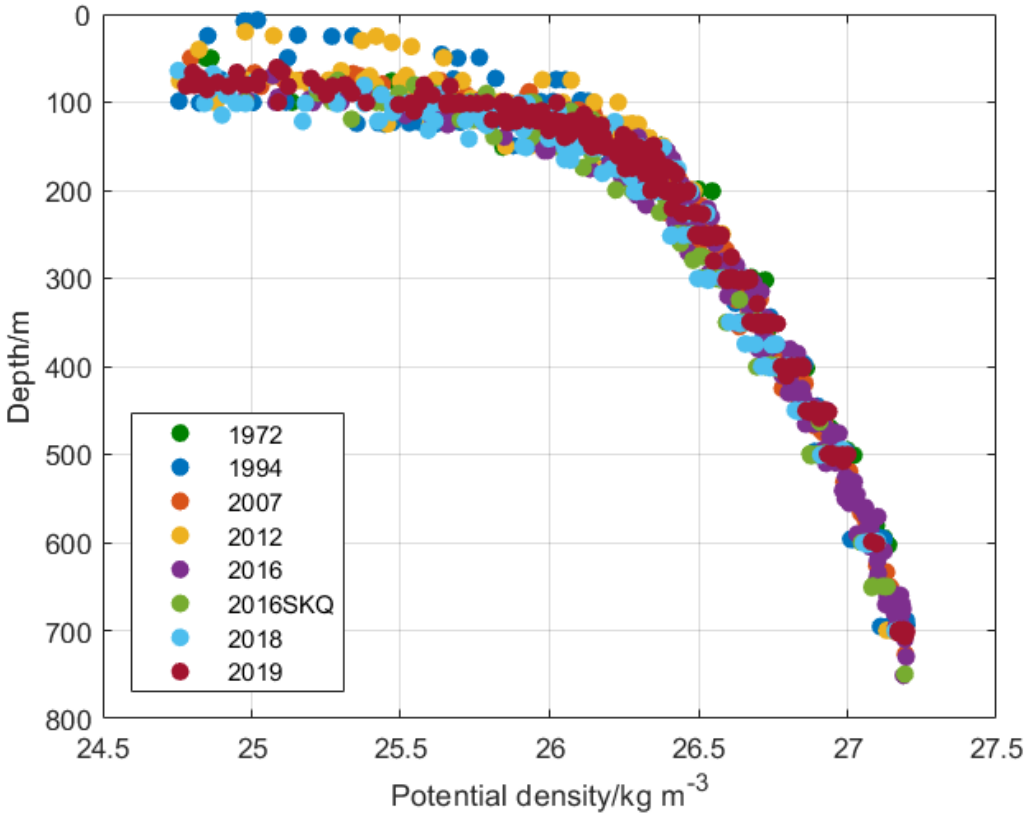

Figure S1. Scatter plot of data from each of the eight cruises in the ETNP ODZ depicting depth versus potential density.

	1972	1994	2007	2012	2016	2016SKQ	2018	2019
24.75-27.2 kg m^{-3}	6.63E6	6.55E6	6.93E6	7.43E6	7.41E6	7.79E6	7.58E6	8.44E6
24.75-26.2 kg m^{-3}	5.84E5	5.20E5	5.87E5	7.24E5	7.14E5	9.03E5	7.60E5	7.58E5
26.2-26.8 kg m^{-3}	2.97E6	2.78E6	3.18E6	3.56E6	3.39E6	3.60E6	3.46E6	3.77E6
26.8-27.2 kg m^{-3}	2.97E6	3.14E6	3.04E6	3.01E6	3.21E6	3.15E6	3.47E6	3.78E6

Table S3. This table presents the results from integrating fixed N loss, as seen in Fig. 4a-c, however, these data are not corrected with the 0.747 scaling factor that was applied for plotting them in Fig. 5a-c.

	ESW	13CW	NEPIW	AAIW	uPSUW	ξ	Weight
θ/ºC	23.28	13.41	9.47	5.53	7.75	n/a	16
S_A/g kg^{-1}	34.52	34.95	34.78	34.70	32.80	n/a	1
PO_4^{3-}/µmol kg^{-1}	0.17	2.33	2.65	3.27	1.13	1	4
NO_3^-/µmol kg^{-1}	0	29.99	35.60	44.80	10.08	-62	6
SiO_4^{2-}/µmol kg^{-1}	1.28	23.50	33.86	83.53	10.33	11.4	14
σ_θ/kg m^{-3}	23.30	26.29	26.74	27.25	25.6	n/a	16

Table S4. Water mass definitions used in extended optimum multiparameter analysis, including anaerobic remineralization and weighting for each parameter.

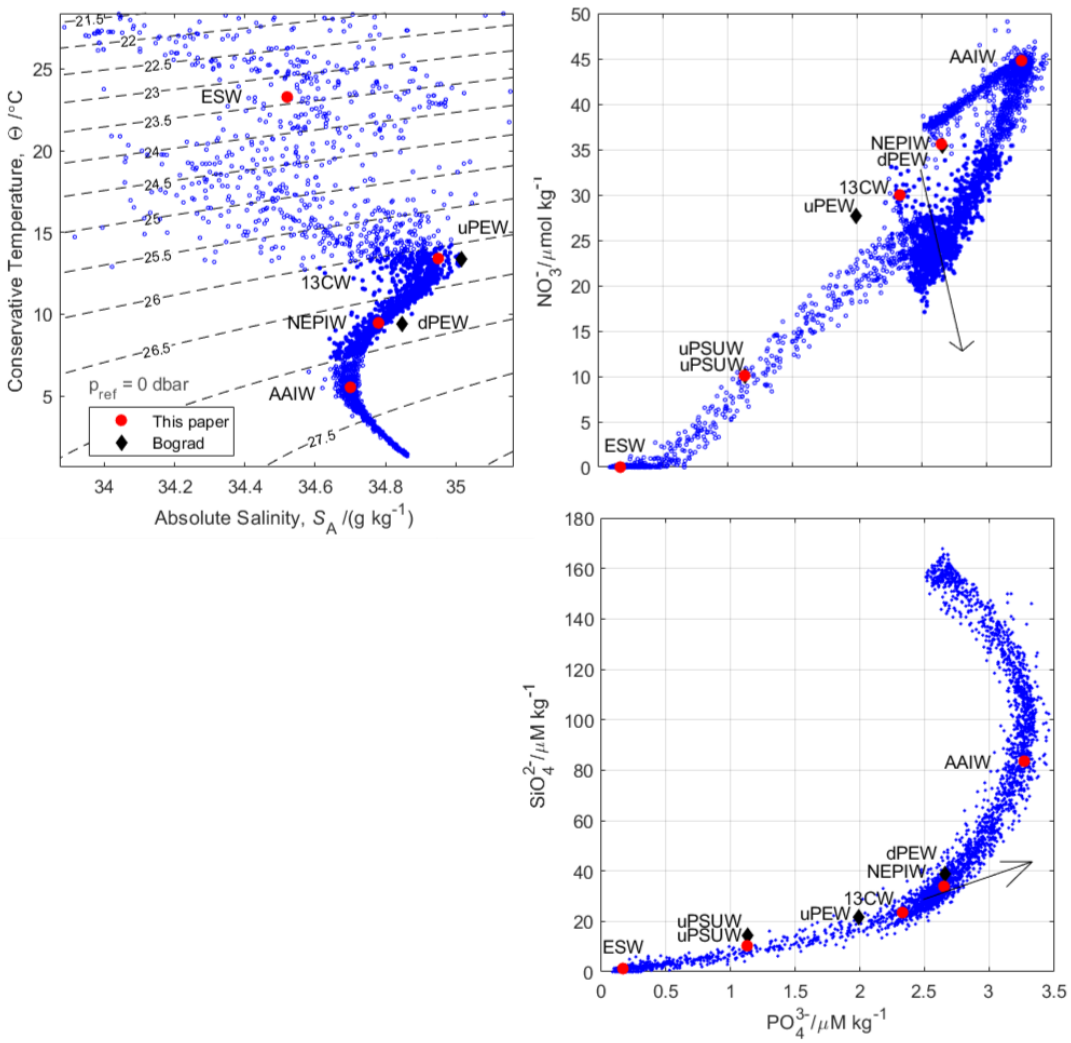

Figure S2. Water mass endmembers, in red diamonds as well as black circles for Bograd et al. (2019), superimposed over the input data to eOMP in blue.

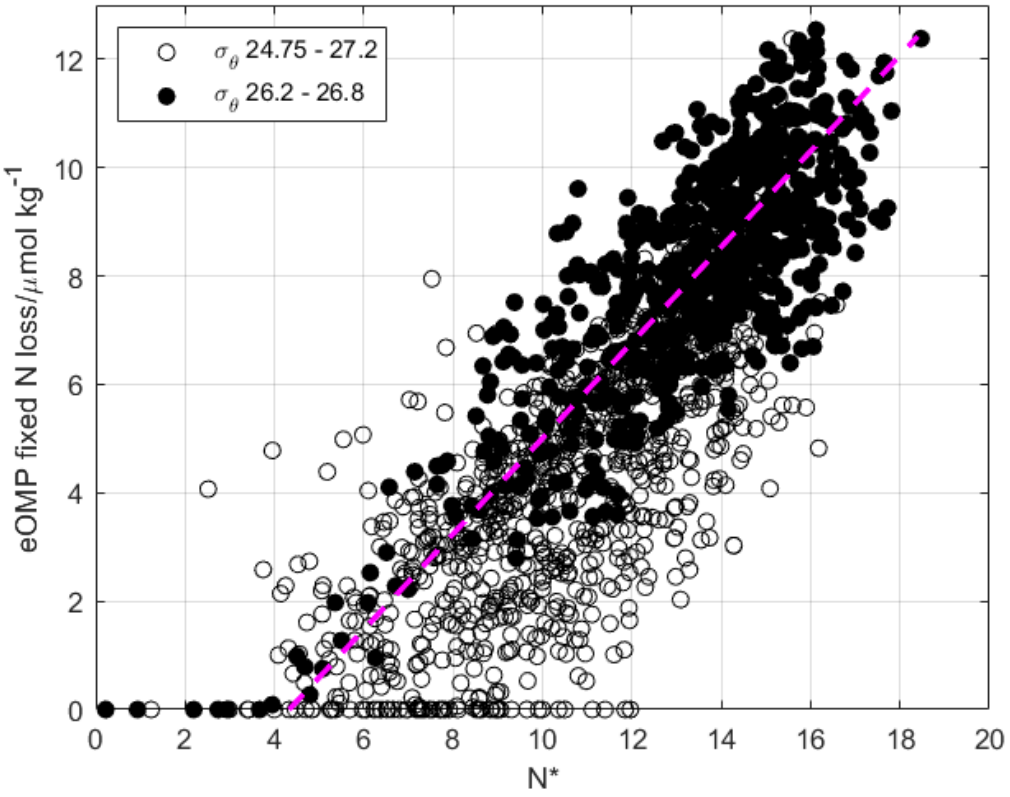

Figure S3. Comparison between N* and eOMP-derived fixed nitrogen loss, described previously as 62ξ.

	Parameter	1972	1994	2007	2012	2016	2016SKQ	2018	2019
26.2-26.8 kg m^{-3}	Mean	10.77	9.43	10.77	11.83	11.02	10.78	11.19	11.79
	Std	0.17	0.65	0.51	0.35	0.59	0.56	0.50	0.42
	n	3	10	9	11	7	7	11	13
26.8-27.2 kg m^{-3}	Mean	8.1	7.92	7.72	7.23	7.29	8.12	8.7	9.74
	Std	1.0	0.44	0.60	0.16	0.67	0.25	1.4	0.48
	n	3	7	6	4	7	2	7	7

Table S5. Mean fixed N loss data, calculated via eOMP, as depicted in Fig. 6a..

	O_2/μM					
Year	Winter	Spring	Summer	Fall	Mean	Standard deviation
1984	83	78	76	74	78	4
1985	68	68	72	71	70	2
1986	78	75	67	86	76	8
1987	86	88	86	87	87	1
1988	88	0	82	85	85	3
1989	79	78	81	91	82	6
1990	0	0	87	98	93	8
1991	95	0	92	90	92	2
1992	90	96	97	92	94	3
1993	98	97	96	99	97	1
1994	102	96	82	95	94	8
1995	102	87	95	87	93	7
1996	92	93	86	87	89	3
1997	88	87	85	74	83	6
1998	99	97	96	0	97	1
1999	88	86	85	87	86	1
2000	86	84	83	84	84	1
2001	87	85	83	86	85	2
2002	85	82	79	83	82	2
2003	84	79	68	80	78	7
2004	84	82	78	82	81	2
2005	82	81	78	71	78	5
2006	77	76	74	79	77	2
2007	80	77	78	70	76	4
2008	72	73	77	77	75	3
2009	75	79	73	82	77	4
2010	87	77	76	71	78	7
2011	77	70	73	73	73	3
2012	70	54	66	74	66	8
2013	75	65	73	77	73	5
2014	42	71	83	84	70	20
2015	0	76	76	76	76	0
2016	86	78	70	80	78	7
2017	81	76	76	80	78	2
2018	0	82	80	82	82	1
2019	0	72	73	81	75	5

Table S6. Mean oxygen concentrations measured on CalCOFI cruises, by each season and year, then the means and standard deviations used in Fig. 6b.

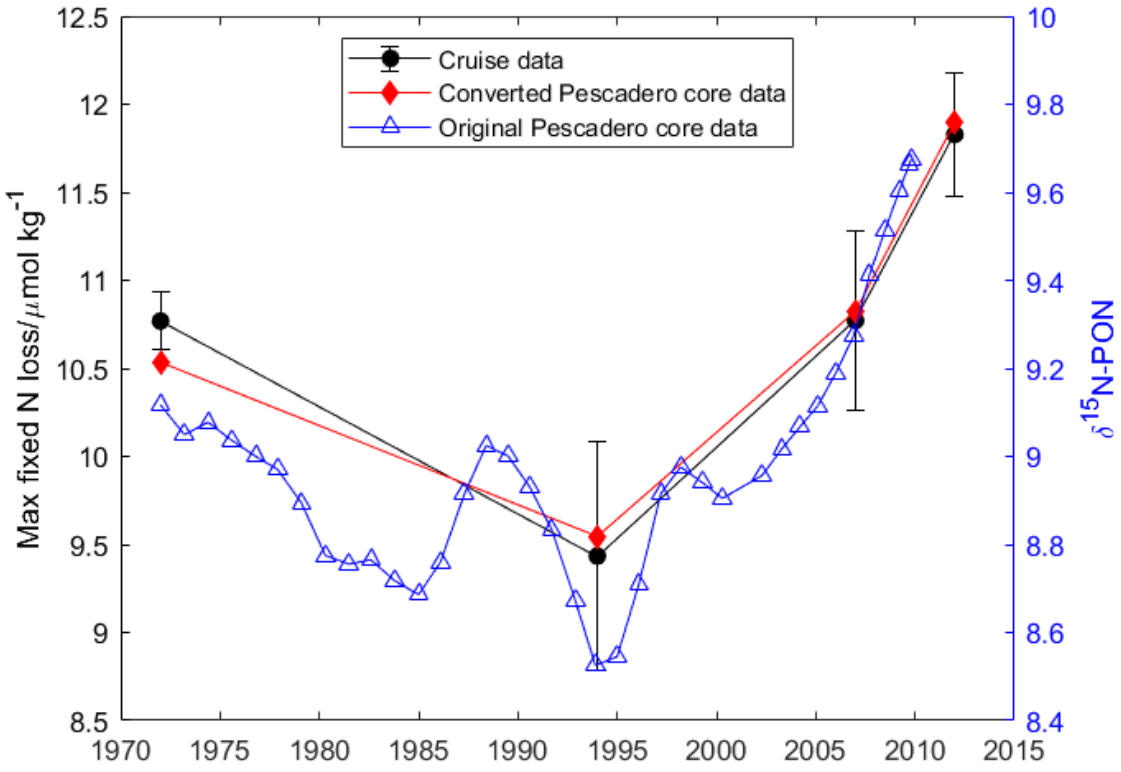

Figure S4. Plot highlighting the four maximum fixed N loss measurements from eOMP calculations (black circles) versus the "rloess" Pescadero basin N isotope data, on the right y-axis, used for conversion. We also display this Pescadero basin data converted to max fixed N loss using m=1.68±0.19 and b=-4.8±1.8 with Eq. 4.

	1972	1994	2007	2012	2016	2016SKQ	2018	2019
Mean	152.1	122.1	119.0	136.6	138.5	147.4	127.2	152.1
Standard deviation	0.76	0.47	1.3	0.52	0.64	1.1	1.7	0.76
Number of samples	11	10	11	11	7	11	11	11

Table S7. Depth of the 13CW water depicted in Fig. 6a, with the number of samples with 13CW as determined from 1-m binned data, the mean depth, and the standard deviation.

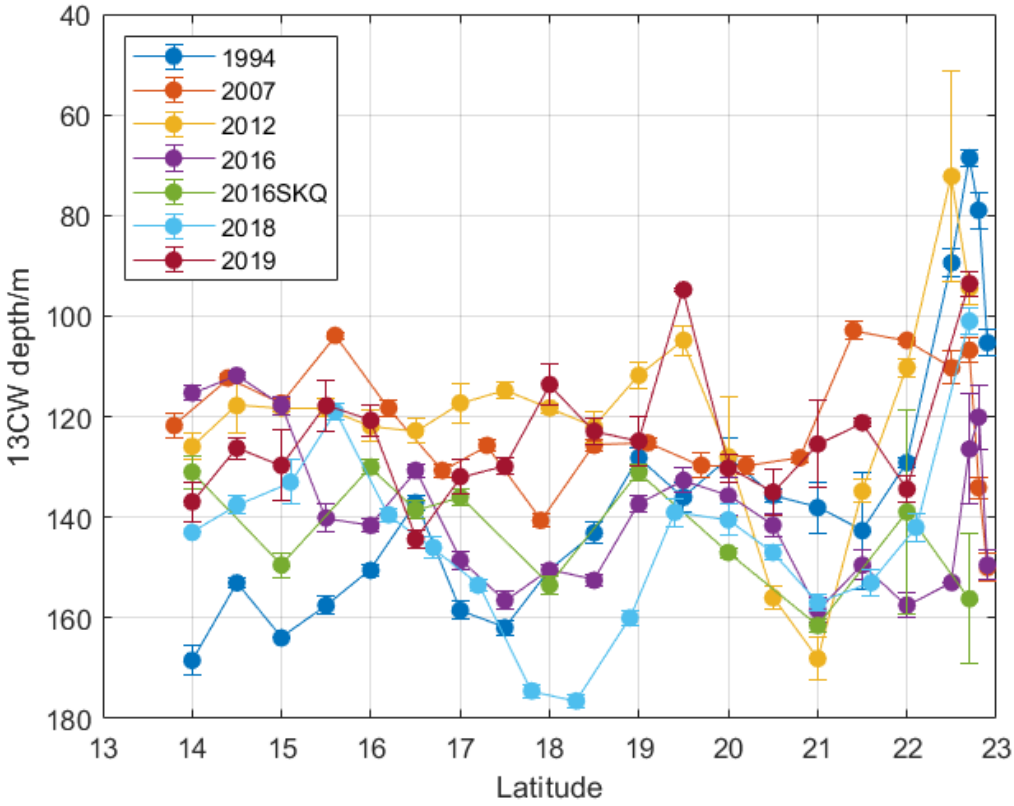

Figure S5. Depth of the 13CW for each station on each expedition. Data between 14 and 19 ºN is used to generate the data in Table S6..

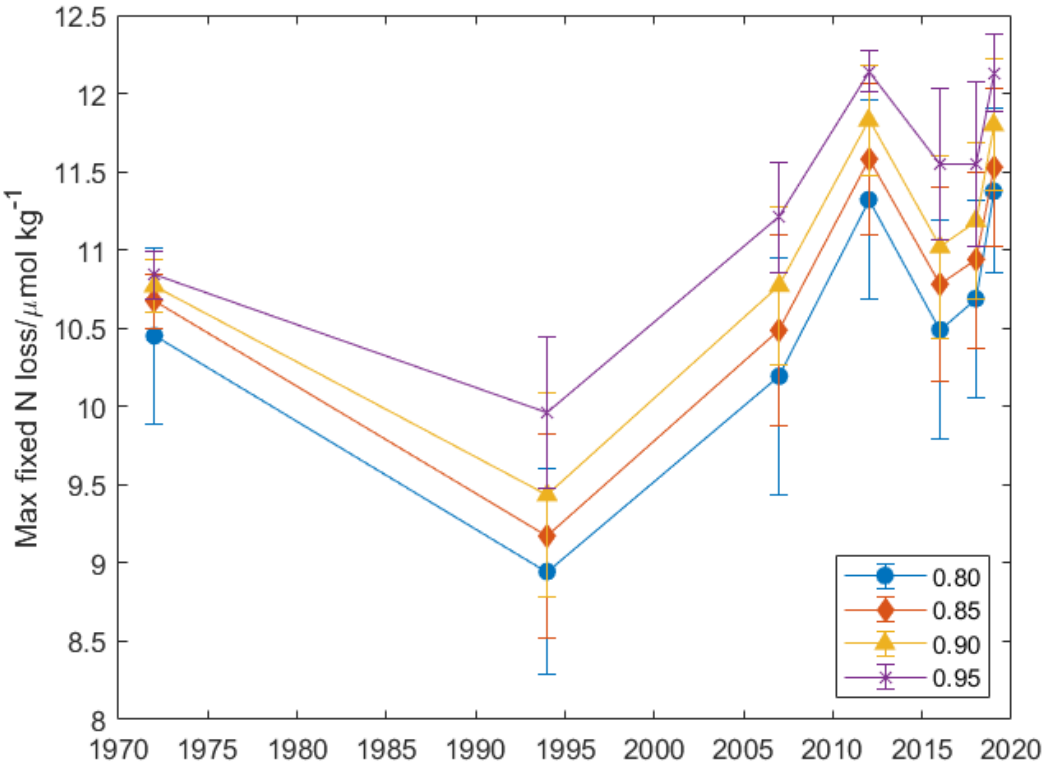

Figure S6. Sensitivity analysis for calculating the strength of the core ETNP ODZ based on quantile. The mean and standard deviation for the 80%, 85%, 90%, and 95% quantile are presented.